Journal of Organometallic Chemistry, 415 (1991) 143–153
Elsevier Sequoia S.A., Lausanne
JOM 21981

Structural studies of organometallic compounds in solution

II *. Magnesium bromide and iodide in diethyl ether and tetrahydrofuran; an extended X-ray absorption fine structure (EXAFS) and large angle X-ray scattering (LAXS) study

Agneta Wellmar [a] and Ingmar Persson [b,*]

[a] *Inorganic Chemistry 1, Chemical Centre, University of Lund, P.O. Box 124, S-221 00 Lund (Sweden)*
[b] *Department of Chemistry, Swedish University of Agricultural Sciences, P.O Box 7015, S-750 07 Uppsala (Sweden)*

(Received March 25th, 1991)

Abstract

The structures of the magnesium iodide complexes formed in concentrated diethyl ether and tetrahydrofuran solutions have been determined by the large angle X-ray scattering (LAXS) technique. Those of the more dilute solutions of magnesium bromide in diethyl ether and tetrahydrofuran solutions have been determined by the extended X-ray absorption fine structure (EXAFS) method. The investigation of the MgI_2 diethyl ether solution was carried out at 44 °C since this solution crystallizes at about 30 °C. This solution is probably best considered a melt, the structure of which can be regarded as a close-packing of iodide ions with magnesium ions occupying some of the holes. The coordination around a specific magnesium ion depends on whether it occupies a tetrahedral or an octahedral hole. The average Mg–I bond distance is 2.75 Å. Solvated MgI^+ is the dominating complex in MgI_2–tetrahydrofuran solution. Magnesium is probably six-coordinate in this complex, and the Mg–I bond distance is 2.52(5) Å. The Mg–Br bond distance is 2.49 and 2.66 Å in diethyl ether and tetrahydrofuran, respectively.

Introduction

This paper provides an introduction to a comprehensive study of the structures of organomagnesium bromides and iodides in diethyl ether and tetrahydrofuran (THF) solution. To be able to estimate the possible presence of MgX_2, and thereby demonstrate the existence of Schlenk equilibria in Grignard systems, the structures of the magnesium halides in diethyl ether and THF solution must be known. The number of structural determinations of magnesium halide complexes is limited. Solid magnesium bromide and iodide have the CdI_2 layer structure, in which

* For Part I see ref. 10.

0022-328X/91/$03.50

magnesium is octahedrally coordinated [1], as is the hydrated magnesium ion [2]. It was therefore of interest to study the coordination chemistry of magnesium halides in more poorly solvating solvents, such as diethyl ether and THF.

The crystal structures of several compounds with Mg–Br bonds have been investigated but in the case of MgI_2 the structural analyses are not quite conclusive. The samples undergo significant decomposition and the X-ray patterns deteriorate [3]. In the reported structures, including those of some Grignard reagents, where diethyl ether is the solvate molecule, a tetrahedral arrangement around the magnesium atom has been established [4–6]. With tetrahydrofuran as the solvate molecule an octahedral arrangement has been reported [7]. The solvating ability of THF is considerably stronger than that of diethyl ether [8]. This implies that the solvation of magnesium(II), and so the degree of dissociation of magnesium halides, is higher in THF than in diethyl ether.

Walker and Ashby concluded from ebullioscopic measurements that the degree of association of $MgBr_2$ and MgI_2 in diethyl ether at infinite dilution is 1; i.e. only monomeric species are present. The degree of association increases with increasing concentration to values of 2.6 and 2.9 at 0.5 *m* for the bromide and the iodide, respectively [9].

We present here the structures of $MgBr_2$ in diethyl ether and THF as determined by extended X-ray absorption fine structure, EXAFS, the structure of MgI_2 in THF (0.88 *M*) as determined by large angle X-ray scattering, LAXS, and a recalculation of previously reported LAXS data on MgI_2 in diethyl ether [10]. All measurements were performed at room temperature, 25 °C, except for MgI_2 in diethyl ether, for which the temperature was 44 °C. A plot of the LAXS raw intensity data against the scattering angle for MgI_2 in both solvents displayed a somewhat curved function, and so a correction had to be made in the data treatment procedure. These data have now been reanalysed by use of another routine; the reanalysed data are of significantly better quality, and a more detailed model of the structure is proposed below.

Experimental

All glass equipment was dried in an oven at approximately 120 °C. All preparations were carried out under dry argon in a glove box. Reaction flasks were opened for sampling in the glove box.

Solvents

The solvents used were either distilled over metallic sodium, with benzophenone as an indicator, or anhydrous ether from Aldrich in Sure/Seal™ bottles were used. The solvents were transferred to reaction flasks with hypodermic syringes.

General preparative procedure

To prepare the diethyl ether solutions of the magnesium halides and the THF solution of $MgBr_2$, the mercuric halide (Fluka) and an excess of magnesium turnings (Merck) were placed in a round-bottomed flask equipped with a condenser, and the solvent was added. The reaction was initiated by heating and the ether was refluxed until all the mercuric halide had reacted. The solutions were filtered to remove unchanged magnesium and the formed magnesium amalgam.

During the preparation of magnesium iodide in diethyl ether a two-phase system was formed. The upper phase is an ordinary diethyl ether solution with a mag-

Table 1

Composition of the solutions investigated

Solution	$[Mg^{2+}]$ (M)	$[X^-]$ (M)	[Solvent] (M)	μ (cm^{-1})
MgI_2 in diethyl ether	2.5	5.0	5.5	26.9
MgI_2 in THF	0.9	1.8	10.6	9.0
$MgBr_2$ in diethyl ether	0.4	0.8		
	0.1	0.2		
$MgBr_2$ in THF	0.2	0.4		

nesium iodide concentration of about 0.2 M. The lower phase is yellowish and fairly viscous, and solidifies at about 30 °C. The magnesium iodide concentration in this phase is 2.50 M and the diethyl ether concentration is 5.45 M, Table 1.

Magnesium iodide is soluble in THF, and the THF solutions were prepared by dissolving the appropriate amount of anhydrous MgI_2.

Analyses

The solutions were analysed for magnesium by titration with EDTA using Eriochrome Black T as indicator, and for halide by titration with a standard $AgNO_3$ solution. The analyses were carried out in aqueous solution.

EXAFS data collection and reduction

X-ray absorption spectra were collected at Stanford Synchrotron Radiation Laboratory, SSRL, and at Daresbury Laboratory Synchrotron Radiation Source, SRS. The spectra for each solution were recorded several times (Table 2). The intensities were measured in transmission mode with nitrogen-filled ion chambers to monitor incident and transmitted radiation. At SRS the ion chambers were filled with the recommended gas mixtures; 19.6 kPa Ar + 81.7 kPa He for the first ion chamber and 15.5 kPa Xe + 85.8 kPa He for the last two ion chambers [11]. The spectra presented are an average of at least 2–3 scans. Energy calibration was carried out by the internal standard technique [21] with solid KBr as reference. The inflection point of the KBr standard was assigned as 13472 eV.

The averaged data were reduced by subtracting a smooth polynomial pre-edge extrapolated from a measured pre-edge, subtracting a cubic spline and normalising [13,14]. The spline points were chosen empirically to minimise the residual low-frequency background without reducing the observed amplitude of the EXAFS. The normalised, background-subtracted EXAFS data were converted from the energy E to the photoelectron wave vector k, $k = [2m_e(E - E_0)/\hbar^2]^{1/2}$, with an E_0 value of 13490 eV. Fourier transforms of the data were calculated by numerical integration with k^3-weighted data. Data reduction for the model compound was performed in exactly the same way as for the solutions.

EXAFS data analyses

The observed EXAFS, $\chi(k)$, can be expressed as

$$\chi(k) = \frac{i \sum N_s F_s(k)\, e^{-2\sigma^2 k^2}\, e^{-2R_{as}/\lambda}}{kR_{as}^2} \sin[2kR_{as} + \alpha_{as}(k)] \qquad (1)$$

Table 2

EXAFS data collection [a]

		Data collection
Solution		
$MgBr_2$ in diethyl ether	0.4 *M*	April 87 December 87
	0.1 *M*	March 89
$MgBr_2$ iN THF	0.2 *M*	April 87 December 87
Model	*Distance (Å)*	
Br_2	Br–Br 2.28	April 87 December 87
CBr_4	Br–C 1.94 Br–Br 3.16	April 87 December 87 August 89
BrO_3	Br–O 1.68	April 87 November 87
$MgBr_2$	Br–Mg 2.70	April 87 November 87 December 87
NaBr	Br–Na 2.99	March 89 August 89

[a] All EXAFS experiments were performed under dedicated conditions (3–3.3 GeV, 40 mA, 16.5–18 kG).
- April 87 - SSRL, beam line 7-3, Si(220) double-crystal monochromator, 8-pole wiggler, unfocussed.
- November 87 - SSRL, beam line 4-2, Si(111) double crystal monochromator, 8-pole wiggler, focussing mirror.
- December 87 - SSRL, beam line 7-3, Si(111) double-crystal monochromator, 8-pole wiggler, unfocussed.
- March 89 - SSRL, beam line 4-1, Si(111) double-crystal monochromator, 8-pole wiggler, unfocussed.
- August 89 - SRS, beam line 9-2, Si(220) double-crystal monochromator, 3-pole wiggler, unfocussed.

where N_i is the number of scatterers in the ith shell, F_i is the photoelectron backscattering amplitude of the ith shell, σ is the Debye–Waller factor which accounts for thermal vibration and static disorder. σ^2 is the mean-square variation in the absorber–scatterer distance R_{as}. λ is the mean-free path length for the photoelectron and $\alpha_{as}(k)$ is the net phase shift in the photoelectron wave during scattering. The sum is taken over all shells of scatterers, where a shell consists of some number of undistinguishable atoms at the same (or undistinguishable) distance from the absorber. Typically, the first shell bond lengths and coordination number can be determined to ± 0.02 Å and $\pm 20\%$, respectively [15,16]. For two shells of the same atomic type the approximate resolving power of EXAFS is $\Delta R > \pi/2k_{max}$. Since k_{max} for EXAFS data is typically 13–17 $Å^{-1}$ this places a lower limit of 0.1 Å on the resolvable distance between shells. In practice the noise in the data results in an effective resolution closer to 0.2 Å.

The curve-fitting procedure that followed data reduction involved fitting the EXAFS of a model compound with a known structure, using a parameterised EXAFS equation. The model compound was chosen such that there was a single

shell of atoms contributing to each peak in the Fourier transform. Fourier-filtering techniques were used to isolate the shell of interest. A six-parameter function was fitted to the measured EXAFS for the model compound [15,17,18]. This parameterised function was then used when fitting the EXAFS of the unknown samples. When fitting the unknown structures the number of scatterers and the absorber–scatterer distance were adjusted as variable parameters. The principal advantage of this approach is the small number of variable parameters per shell and the corresponding decrease in parameter correlation problems. This method of analysis makes use of the fact that the amplitude and phase parameters are reasonably transferable from compound to compound [16], provided that the chemical environments are similar.

All calculations were performed by the computer program package XFPAKG [19].

LAXS data collection

The collection of LAXS data has been described previously [10].

Treatment of LAXS data

The experimental data were initially corrected for background scattering and polarisation effects [20]. Correction for multiple scattering was made because of the low absorption coefficients [21], Table 1. The corrected data were normalised to a stoichiometric volume containing one magnesium atom. The normalisation factor, K, used in the data analysis was derived by comparison of the measured and total independent scattering in the high-angle region, $s > 13$ Å^{-1}. K calculated in this manner [22] was then compared with K calculated according to the method described by Krogh-Moe [23] and Norman [24].

Scattering factors, f, for the neutral atoms were used [25] except for H, for which the spherical form factors suggested by Stewart et al. were employed [26]. The contribution from anomalous dispersion, $\Delta f'$ and $\Delta f''$, was considered for all atoms [25]. Incoherent scattering factors [27–29], corrected for the Breit–Dirac effect [30,31], were used. The raw data were normal up to about $s \approx 10$ Å^{-1}, where an unexpected decrease in the total intensity was observed. In this previous paper successive Fourier transformations were used to straighten up the intensity function. These repeated Fourier transformations influenced the data and thereby the result, in a negative way. It was later found that a better way to straighten up the function without interfering with the structural information in the intensity function, was to apply a smoothed correction function to the experimental function. After this correction one Fourier transformation was enough to straighten out the entire experimental function, as is the normal case with good raw data. All these corrections were taken into account when the reduced intensity function, $i(s)$, and the differential radial distribution function, $D(r) - 4\pi r^2\rho_0$, was calculated using standard procedures [32]. Spurious peaks below 1.5 Å which could not be identified with interatomic distances in the solutions were removed by a Fourier transformation procedure [33].

All calculations were made with the program KURVLR [34]. Least-squares refinements were carried out using the STEPLR program [35].

Results

EXAFS data were collected on several occasions, Table 2. Data were not usable beyond $k \approx 13$ Å^{-1} when Si(220) crystals were used, because of a monochromator defect. With Si(111) crystals the data are usable out to $k \approx 15$ Å^{-1}, but even with this increased data range the Br–Br interaction was not revealed. The unfiltered EXAFS data are given in Fig. 1. The model compound data used are those collected at SSRL. The monochromator problem made it impossible to extract reliable parameters from the data collected at SRS.

Originally, the model compound of choice was $MgBr_2$(s) and data for this were determined repeatedly. However, owing to the hygroscopicity of this compound the scans were not reproducible and the individual scans could not be averaged. Parameters were extracted from NaBr(s) instead.

EXAFS of $MgBr_2$ in diethyl ether

The Fourier transforms show a single peak at a distance corresponding to 2.5 Å, Fig. 2. At these low concentrations monomeric compounds and perhaps formation

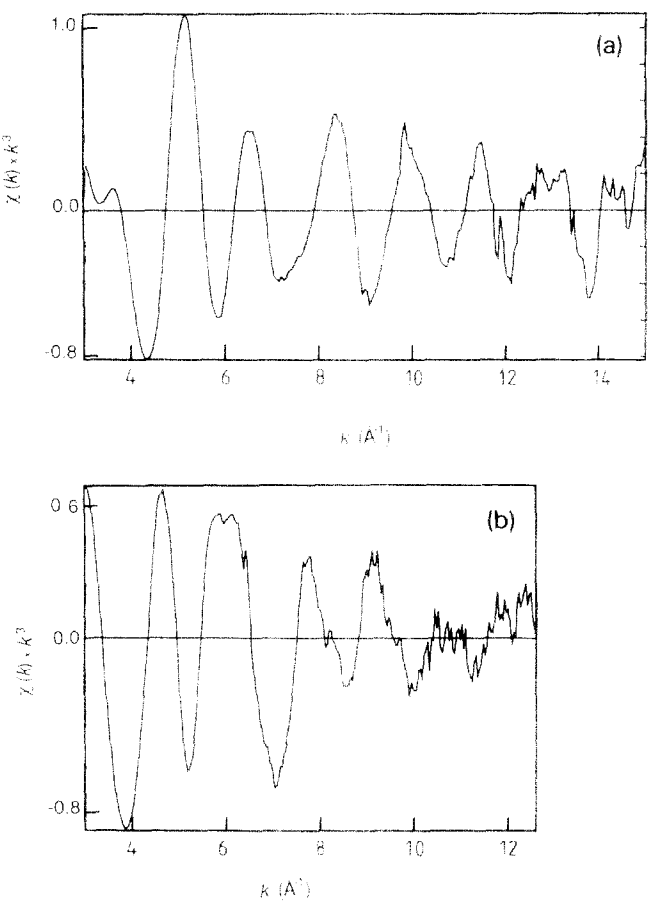

Fig. 1. EXAFS, $\chi(k)$, multiplied by k^3 vs k of magnesium bromide in (a) diethyl ether and (b) tetrahydrofuran solution.

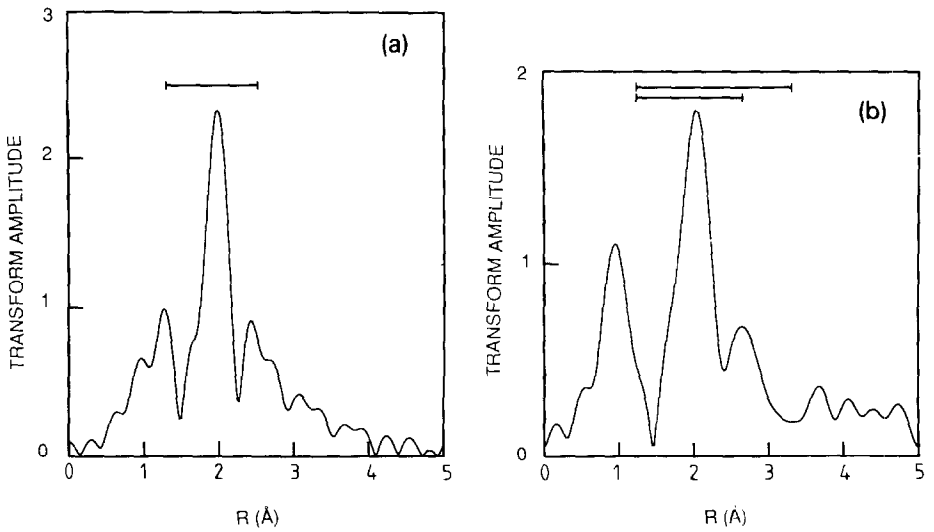

Fig. 2. Fourier transforms of k^3-weighted EXAFS data of magnesium bromide in (a) diethyl ether, k-range 3.0–14.5 $Å^{-1}$, and in (b) tetrahydrofuran, k-range 3.0–12.7 $Å^{-1}$, (b). The horizontal bars indicate the width of the windows used when back-transforming the data. R is related to the true distance R' by the phase shift α according to $R' = R + \alpha$.

of dimers are to be expected. However, there are no signs of a Br–Br interaction in the transforms. The Br–Mg peak was filtered, and after back-transformation the curve-fitting gave a Br–Mg distance of 2.49 Å, Table 3.

EXAFS of $MgBr_2$ in THF

The Fourier transform for this solution also shows a single peak but with a lower intensity than for the diethyl ether solution, Fig. 2. The fits did not give reliable coordination numbers, but the $MgBr_2$ is probably dissociated and the peak is due to magnesium backscattering in a $MgBr^+$ ion. Curve-fitting this peak gave a Mg–Br distance of 2.66 Å, Table 3. A smaller peak at 2.6 Å in the Fourier transform was also included in a wider filter. The extracted wave from the wider filter was not much different from the wave corresponding to the first peak. The smaller peak could not be fitted.

LAXS of MgI_2 in diethyl ether

In the radial distribution function, RDF, there are two peaks at 2.7 and 4.5 Å, and one marked shoulder at 3.9 Å, Fig. 4. There is also a small peak around 1.5 Å

Table 3

EXAFS curve-fitting results of magnesium bromide in diethyl ether and THF solutions

Compound	Conc. (M)	Br–Mg distance (Å)	
		k = 3–12.7 ($Å^{-1}$)	k = 3–14.5 ($Å^{-1}$)
$MgBr_2$ in diethyl ether	0.4	2.50	
	0.1		2.49
$MgBr_2$ in THF	0.2	2.66	

Table 4

Interatomic distances, d (Å), temperature coefficients, b (Å^2), and number of distances, n. Errors derived from least-squares minimisations are shown in parentheses

Interaction	Parameter	MgI_2 in diethyl ether	MgI_2 in THF
Mg–I	d	2.75, 5.25, 6.05	2.52(5)
	b	0.008, 0.025, 0.025	0.008
	n	1.67, 2.0, 2.0	1.0
I–I	d	3.88, 4.52, 7.90, 8.50, 11.50, 12.10	
	b	0.025, 0.025, 0.030, 0.030, 0.035, 0.035	
	n	1.0, 1.5, 1.0, 0.67, 0.33, 0.5	
Mg–O	d	2.15	2.81
	b	0.010	0.010
	n	3.0	5.0

and this was assigned to intramolecular C–O and C–C distances in diethyl ether of 1.408 and 1.516 Å, respectively. The peak at 2.7 Å contains a Mg–I distance as well as the intramolecular diethyl ether C–O and C–C distances at 2.47 and 2.43 Å, respectively.

The series of distances at 2.7, 3.9 and 4.5 Å may indicate that the magnesium–iodide distances are 2.7 Å and that the magnesium ions are surrounded both tetrahedrally and octahedrally by iodide ions, see Fig. 4; the iodides are the only atoms with sufficient scattering power to give rise to such intense peaks that far out in the RDF. The peak at 4.5 Å corresponds to an I–I distance in a tetrahedral configuration of iodides around a magnesium ion. An I–I distance of 4.5 Å corresponds to a Mg–I distance of 2.75 Å when the iodides are at the corners of a

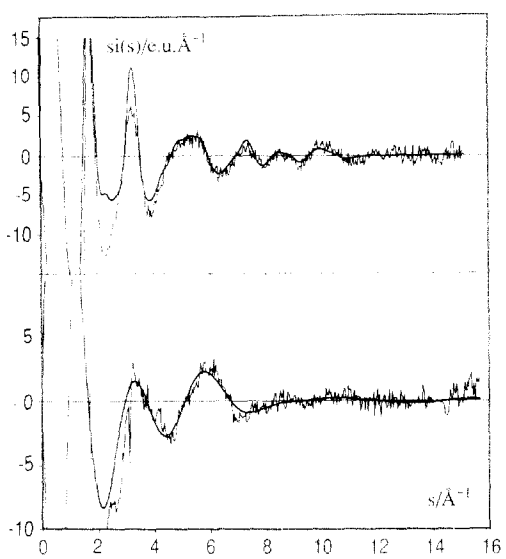

Fig. 3. Reduced intensities, $i(s)$, multiplied by s vs s for magnesium iodide in diethyl ether (upper) and tetrahydrofuran (lower) solution. Experimental values are represented by the thin lines and the values calculated from the final structure model in Table 4 by the thick lines.

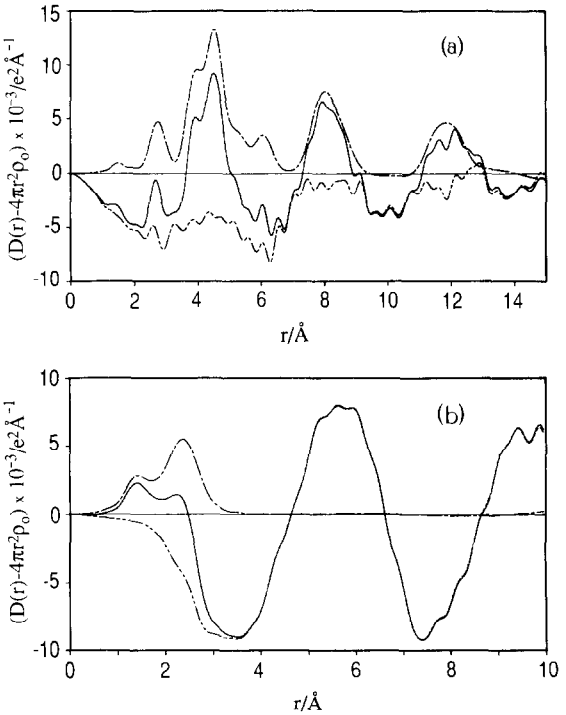

Fig. 4. The differential electronic radial distribution function $D(r)-4\pi r^2\rho_0$ functions for magnesium iodide in (a) diethyl ether and (b) tetrahydrofuran solution, solid lines. The dashed lines represent the sum of the calculated peak shapes and the difference is drawn with double-dashed lines.

tetrahedron. In an octahedral configuration an I–I distance of 3.9 Å also gives a Mg–I distance of 2.75 Å. The intensity of the peak at 4.5 Å corresponds to about 1.5 I–I distances per magnesium, and the shoulder at 3.9 Å corresponds to roughly one I–I distance per magnesium.

The very concentrated diethyl ether solution of magnesium iodide contains only about two solvent molecules per magnesium iodide. The solution can therefore be regarded as a melt of iodide and magnesium ions. Whether the solvent molecules are coordinated to the magnesium or evenly distributed in the solution cannot be determined by the LAXS technique used in this study. The structure of this melt can be regarded as close-packing of iodide ions with magnesium ions occupying some of the holes, as can be seen from the number of Mg–I distances and the stoichiometry. The intensity of the I–I peaks at 3.9 and 4.5 Å, corresponding to I–I distances around octahedral and tetrahedral holes, respectively, shows the ratio of occupied tetrahedral and octahedral holes in the close-packing to be around 1.5. The fit of the theoretical and experimental intensity functions is given in Fig. 3.

LAXS of MgI_2 in THF

There are two peaks in the RDF at 1.5 Å and 2.5 Å. These peaks correspond to intramolecular distances in the THF molecule [36]. In the peak at 2.5 Å there is a Mg–I contribution from a magnesium iodide species and this interaction was refined to 2.52(5) Å, As no I–I interaction is seen in the RDF, MgI_2 is probably

dissociated into solvated MgI^+ and I^- ions, where magnesium is octahedrally coordinated by one iodide ion and five THF molecules. The fit of the calculated and experimental intensity functions is given in Fig. 3.

Discussion

The diethyl ether solution studied is probably best considered a melt of iodide and magnesium ions since there are hardly any free solvent molecules in the solution. The total diethyl ether concentration in the solution is 5.45 *M*, and the concentrations of iodide and magnesium ions are 5.00 and 2.50 *M*, respectively. This means that the diethyl ether present in the solution can hardly act as a solvent in its true sense. Whether diethyl ether is coordinated to the magnesium ions or evenly distributed among the ions cannot be decided from the results of this study. Another indication that this solution should be regarded as a melt is its insolubility in pure diethyl ether. Ionic species cannot be dissolved in diethyl ether due to its low dielectric constant.

The structural information implies that there is a high degree of order in the studied solution/melt as there are large, broad, fairly intense peaks far out in the RDF at 4.5, 8 and 12 Å. The size of these peaks shows that they represent I–I distances. The iodide ions thus seem to be close-packed with the substantially smaller magnesium ions in the holes. The tetrahedral as well as the octahedral holes give Mg–I distances of 2.75 Å, and so it is impossible to determine the distribution of the magnesium ions in the tetrahedral and octahedral holes in the close-packing. This means that the coordination around a specific magnesium ion is determined by the type of hole in the close-packing of iodide ions that it occupies.

The EXAFS data gave no indication of a Br–Br interaction in either solution. For the THF solution this can easily be explained since $MgBr_2$ most probably has dissociated into $MgBr^+$, Br^-, and perhaps also Mg^{2+}. For the diethyl ether solution such an interaction would be expected if the structure is similar to MgI_2 in this solvent. The fact that it is not seen could be due to a large Debye–Waller factor, σ; i.e. the peak in the Fourier transform is broadened and diminished. The Br–Br interaction was still not revealed when the outer data range was increased from $k \approx 13$ to $k \approx 15$ Å^{-1}.

Acknowledgments

This work was supported by the Swedish Natural Science Research Council. The EXAFS measurements were performed at the Stanford Synchrotron Radiation Laboratory, which is supported by the US Department of Energy, Office of Basic Energy Sciences, Division of Chemical Sciences; and the National Institutes of Health, Biomedical Resource Technology Program, Division of Research Resources. XFPAKG was kindly provided by Prof. R.A. Scott. Knut and Alice Wallenberg's Foundation is thanked for support to the LAXS instrument. A.W. thanks Prof. K.O. Hodgson for financial support and for providing the experimental facilities at Stanford University. Dr Britt Hedman's help in performing the EXAFS experiments is gratefully acknowledged.

References

1 A.F. Wells, Structural Inorganic Chemistry, 5th ed., Clarendon Press, Oxford, UK, 1984, pp. 413 and 674.

2 R. Caminiti, G. Licheri, G. Piccaluga and G. Pinna, Chem. Phys. Lett., 61 (1979) 45; idem, J. Appl. Crystallogr., 12 (1979) 34.
3 B.M. Bulychev, K.N. Semenenko, V.N. Verbetskii and K.B. Bitsoev, Moscow Univ. Chem. Bull., 16 (1975) 45.
4 G.D. Stucky and R.E. Rundle, J. Am. Chem. Soc., 86 (1964) 4825.
5 L.J. Guggenberger and R.E. Rundle, J. Am. Chem. Soc., 90 (1968) 5375.
6 H. Schibilla and M.-T. Le Bihan, Acta Crystallogr., 23 (1967) 332.
7 M.-C. Pérucaud and M-T. Le Bihan, Acta Crystallogr., Sect. B, 24 (1968) 1502.
8 I. Persson, M. Sandström and P.L. Goggin, Inorg. Chim. Acta, 129 (1987) 183 and references therein.
9 F.W. Walker and E.C. Ashby, J. Am. Chem. Soc., 91 (1969) 3845.
10 A. Ericson and I. Persson, J. Organomet. Chem., 326 (1987) 151.
11 C. Morrel, J.T.M. Baines, J.C. Campbell, G.P. Diakun, B.R. Dobson, G.N. Greaves and S.S. Hasnain, Daresbury Laboratory Synchrotron Radiation Source's EXAFS Users' Manual, 1988.
12 R.A. Scott, J.E. Hahn, S. Doniach, H.C. Freeman and K.O. Hodgson, J. Am. Chem. Soc., 104 (1982) 5364.
13 J.F. Ahlberg, E.N. Nilsson and J.L. Walsh, The Theory of Splines and Their Application, Academic Press, New York, 1967.
14 F.W. Lytle, D.E. Sayers and E.. Stern, Phys. Rev. B. 11 (1975) 4825.
15 S.P. Cramer and K.O. Hodgson, Prog. Inorg. Chem., 25 (1979) 1.
16 P.A. Lee, P.H. Citrin, P. Eisenberger and B.M. Kincaid, Rev. Mod. Phys., 53 (1981) 769.
17 S.P. Cramer, J.H. Dawson, K.O. Hodgson and L.P. Hager, J. Am. Chem. Soc., 100 (1978) 7282.
18 T.K. Eccles, Doctoral Thesis, Stanford University, USA, 1977.
19 EXAFS data analysis software package, T.K. Eccles, Stanford University and R.A. Scott, University of Georgia.
20 G. Johansson, Acta Chem. Scand., 20 (1966) 553.
21 B.E. Warren, X-ray Diffraction, Addison-Wesley, Reading, MA, 1969, Ch. 10.
22 J.F. Karnicky and C.J. Pings, Adv. Chem. Phys., 34 (1976) 57.
23 J. Krogh-Moe, Acta Crystallogr., 9 (1956) 951.
24 N. Norman, Acta Crystallogr., 10 (1957) 370.
25 International Tables of Crystallography, Kynoch Press, Birmingham, UK, Vol. 3, 1968, and Vol. 4, 1974.
26 R.F. Stewart, E.R. Davidsson and W.T. Simpson, J. Chem. Phys., 42 (1965) 3175.
27 D.T. Cromer and J.B. Mann, J. Chem. Phys., 47 (1967) 1892.
28 D.T. Cromer, J. Chem. Phys., 50 (1969) 4857.
29 A.H. Compton and S.K. Allison, X-ray in Theory and Experiment, van Nostrand-Reinhold, New York, 1935.
30 G. Breit, Phys. Rev., 27 (1926) 362.
31 P.A.M. Dirac, Proc. R. Soc. London, 4 (1926) 195.
32 M. Sandström and G. Johansson, Acta Chem. Scand., Ser. A, 31 (1977) 132.
33 H.A. Levy, M.D. Danford and A.H. Narten, Data Collection and evaluation with X-ray Diffractometer Designed for the Study of Liquid Structure, Report ORNL-3690, Oak Ridge National Laboratory, Oak Ridge, 1966.
34 G. Johansson and M. Sandström, Chem. Scr., 4 (1973) 195.
35 M. Molund and I. Persson, Chem. Scr., 25 (1985) 197.
36 A. Almenningen, H.M. Seip and T. Willadsen, Acta Chem. Scand., 23 (1969) 2748.